Table 1. Clinical Parameters for MH Patients

Case No./Age (y)/Sex	MH Stage	Preop BCVA	Postop BCVA	ILM Peeling	Postop Retinal Status	Lens Status Preop/Postop	Postop IOP Elevation	Complication	Follow-up (mo)
1/58/F	3	20/63	20/20	+	MH closed	Phakic/IOL	−	None	9
2/77/M	4	20/200	20/200	+	MH closed	Phakic/IOL	−	None	8
3/57/F	3	20/50	20/32	+	MH closed	Phakic/IOL	−	None	7
4/62/F	2	20/100	20/25	+	MH closed	Phakic/IOL	−	None	7
5/68/M	3	20/100	20/40	+	MH closed	Phakic/IOL	−	Peripheral retinal break	7
6/79/M	3	20/80	20/50	+	MH closed	IOL/IOL	−	Peripheral retinal break	7
7/78/M	3	20/125	20/25	+	MH closed	Phakic/IOL	+	None	7
8/63/F	3	20/50	20/20	+	MH closed	Phakic/IOL	−	None	7
9/64/F	2	20/63	20/25	+	MH closed	Phakic/IOL	−	None	7
10/73/M	4	20/200	20/50	+	MH closed	Phakic/IOL	−	None	6

MH, macular hole; preop, preoperation; BCVA, best-corrected visual acuity; postop, postoperation; ILM, internal limiting membrane; IOP, intraocular pressure; +, present; IOL, intraocular lens; -, absent.

In this study, we investigated the staining pattern of the membranes and clinical outcome using BBG in macular hole (MH) and epiretinal membrane (ERM) cases. This study was designed as an interventional, noncomparative, prospective, clinical case series.

Methods

Twenty eyes from 20 consecutive patients presenting with MH (10 eyes from 10 patients; 5 men and 5 women) or ERM (10 eyes from 10 patients, 5 men and 5 women) underwent vitrectomy with removal of the membranes using BBG staining solution between August and November 2004. Patients with ocular diseases such as glaucoma, diabetic retinopathy, uveitis, and corneal disorder were excluded. The mean age ± SD of the patients was 67 ± 11.9 years (range, 33–85 years). The mean follow-up ± SD was 7.3 ± 1.0 months. Patient characteristics are summarized in Tables 1 and 2. Preoperative and postoperative ophthal-

mic examinations included slit-lamp microscopy, ophthalmoscopy, and determinations of best-corrected visual acuity (BCVA) and intraocular pressure. MH closure and measurement of foveal thickness (ERM cases) were determined by optical coherence tomography (OCT3; Humphrey Instruments, San Leandro, CA). The mean foveal thickness was calculated from a total of four scans.

Excised specimens from four eyes (two eyes of MH patients and two eyes of ERM patients) were submitted for transmission electron microscopy to verify the presence of ILM. The specimens were postfixed in veronal acetate buffer osmium tetroxide (2%), dehydrated in ethanol and water, and embedded in Epon (Epon 812 Resin, CHIYODA JYUNYAKU INC., Tokyo, Japan). Ultrathin sections were cut from blocks and mounted on copper grids. The specimens were observed with a JEM 100CX electron microscope (JEOL, Tokyo, Japan).

Table 2. Clinical Parameters for ERM Patients

Case No./Age (y)/Sex	ERM Status	Preop BCVA	Postop BCVA	ILM Peeling	Retinal Thickness Preop/Postop (μm)	Lens Status Preop/Postop	Postop IOP Elevation	Complication	Follow-up (mo)
1/33/M	Secondary	20/63	20/32	+	759/232	IOL/IOL	−	None	9
2/85/M	Primary	20/50	20/32	+	441/248	Phakic/IOL	−	None	9
3/72/F	Primary	20/63	20/50	+	423/354	Phakic/IOL	−	None	8
4/85/M	Primary	20/63	20/32	+	478/266	Phakic/IOL	−	Vitreous bleeding	8
6/66/F	Primary	20/40	20/12.5	+	501/240	Phakic/IOL	−	None	7
6/72/M	Primary	20/40	20/16	+	417/190	Phakic/IOL	−	None	7
7/63/F	Primary	20/63	20/25	+	429/232	Phakic/IOL	−	None	7
8/69/F	Primary	20/100	20/100	+	556/382	Phakic/IOL	−	None	6
9/56/M	Pseudo MH	20/40	20/20	+	228/146	Phakic/IOL	−	None	6
10/60/F	Primary	20/40	20/25	+	315/204	IOL/IOL	−	None	6

ERM, epiretinal membrane; preop, preoperation; BCVA, best-corrected visual acuity; postop, postoperation; ILM, internal limiting membrane; IOP, intraocular pressure; +, present; IOL, intraocular lens; -, absent; MH, macular hole.

Fig. 1. Brilliant blue G (BBG)–assisted internal limiting membrane (ILM) peeling for macular hole (MH). The prepared BBG solution (0.25 mg/mL) was injected gently into the vitreous cavity (A) and washed out immediately with balanced salt solution. In MH cases, the ILM was stained a light blue color instantly. The edge and flap of the ILM were clearly visible during the ILM peeling (B and C). After ILM removal, the difference of the retinal surface between the area from which the ILM had been removed and the surrounding area was clearly visible (arrowheads; D).
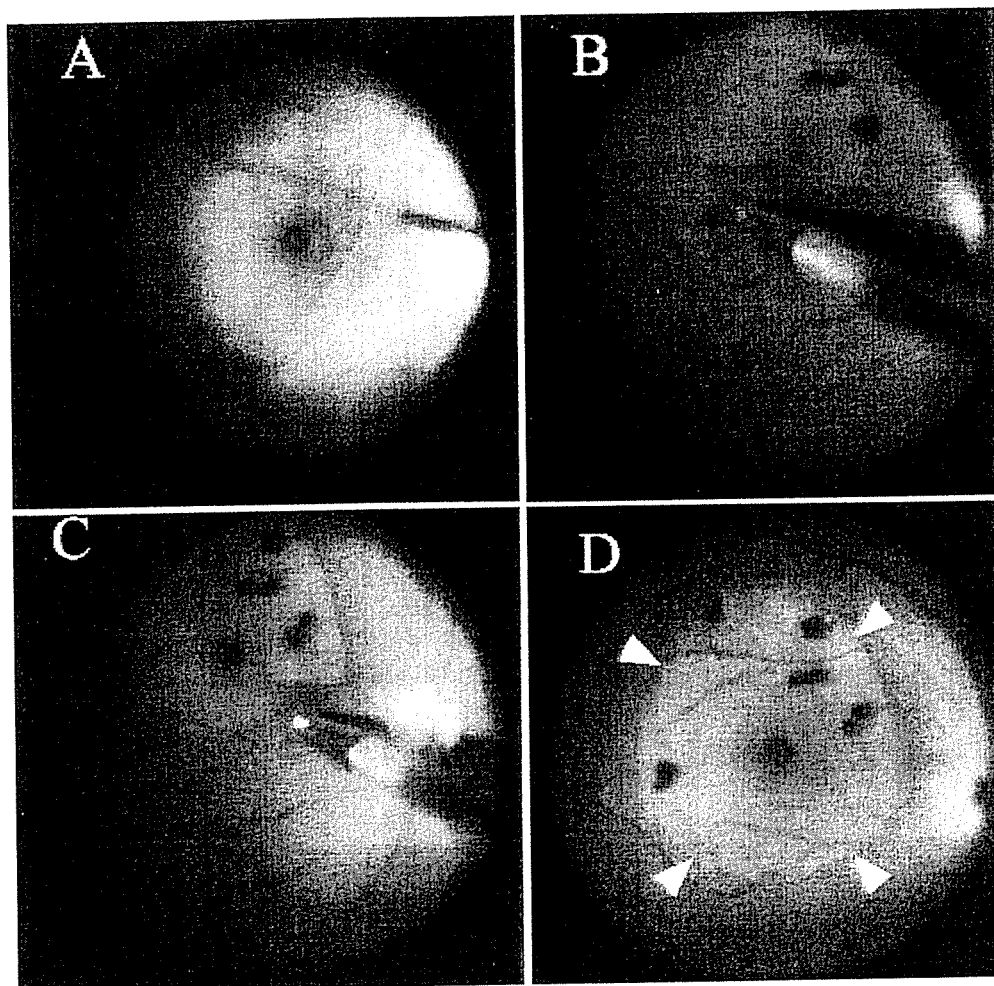
This study was carried out with approval from the institutional review board and performed in accordance with the ethical standards of the 1989 Declaration of Helsinki. The possible advantages and risks of the present treatment were explained to all patients before surgery, and written informed consent was obtained from the patients.

Surgical Technique

Standard phacoemulsification was performed when needed. Surgery consisted of three-port pars plana vitrectomy with induction of a posterior vitreous detachment by suction with a vitrectomy cutter using triamcinolone acetonide injection (Kenakolt-A; Bristol Pharmaceuticals KK, Tokyo, Japan) as required.[19–21] BBG (brilliant blue G 250; Sigma–Aldrich, St. Louis, MO) was dissolved in intraocular irrigating solution (OPEGUARD-MA; Senjyu Pharmaceutical, Osaka, Japan). The solution was then sterilized through a 0.22-μm syringe filter.[22,23] The final concentration of BBG was 0.25 mg/mL (289 mosm;

pH = 7.44). The prepared BBG solution (0.5 mL) was then injected gently into the vitreous cavity (Fig. 1A) and washed out immediately with balanced salt solution (BSS plus; Santen, Osaka, Japan). In MH cases, the ILM was stained a bright blue color instantly. Removal of the ILM was performed using ILM forceps (Fig. 1, B and C). After ILM removal, the difference in the retinal surface color between the area from which the ILM had been removed and the surrounding area was clearly visible (Fig. 1D). In ERM cases, however, staining of the ERM could not be confirmed at this concentration (Fig. 2A). After ERM peeling (Fig. 2B), BBG solution was injected again, followed by immediate irrigation of the vitreous cavity. The ILM of the area where the ERM had been removed was well stained with BBG (Fig. 2C). However, the area where residual ERM and posterior vitreous remained was not stained. The well stained ILM could be easily removed with unstained residual ERM and posterior vitreous (Fig. 2D).

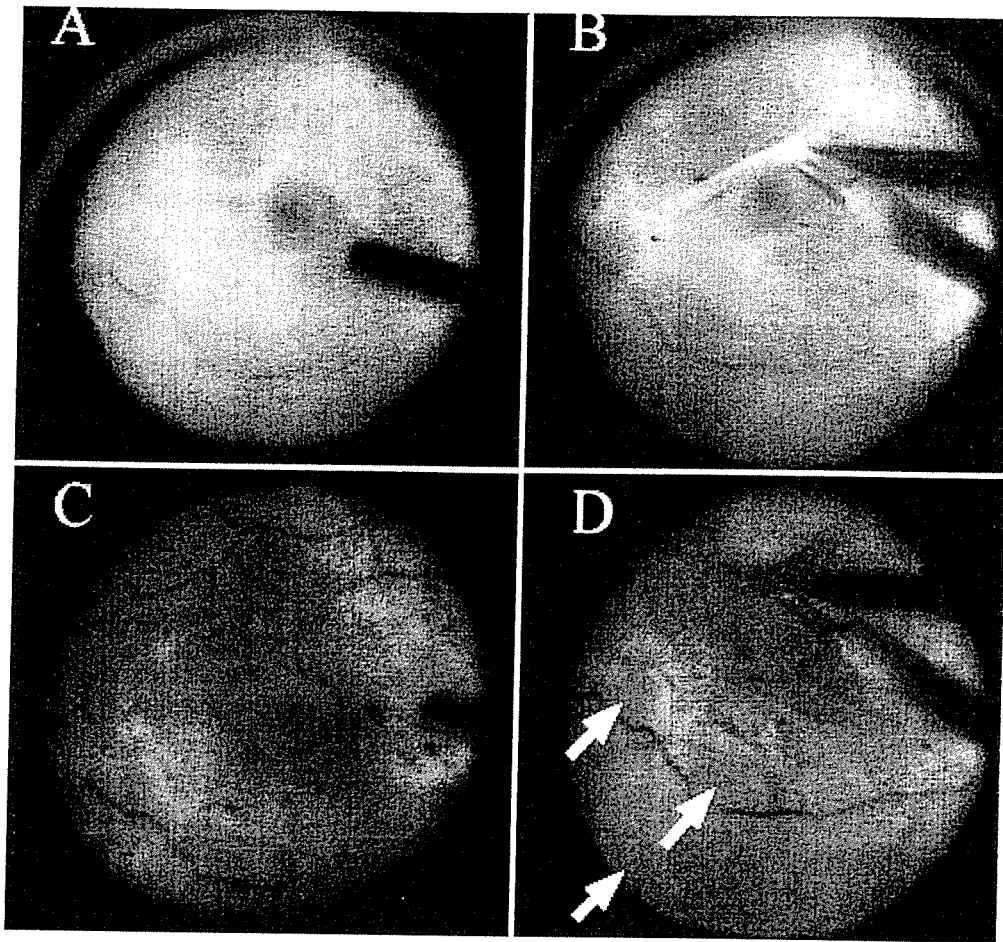Finally, intraocular lenses were inserted in all cases.

Fig. 2. Brilliant blue G (BBG)-assisted membrane peeling for epiretinal membrane (ERM). Staining of the ERM could not be confirmed at this concentration (A). After peeling of the ERM (B), BBG solution was injected again, and the vitreous cavity was irrigated immediately. The internal limiting membrane (ILM) of the area from which the ERM had been removed was well stained (C). The arrows show that the area where residual ERM and the posterior vitreous remained was not stained. The well stained ILM was easily removed (D).

In MH cases, fluid–gas exchange was performed and was replaced with 15% sulfur hexafluoride gas. Patients were advised to maintain a face down posture for 1 week.

Results

The ILM including the ERM was removed from all 20 eyes successfully during surgery. Transmission electron microscopy confirmed the presence of the ILM in all processed specimens (n = 4) (Fig. 3). Postoperatively, any acute toxicity induced by BBG injection, such as corneal edema, severe retinal edema, and severe intraocular inflammation such as endophthalmitis, was not observed by slit-lamp microscopy and ophthalmoscopy by day 14.

All MHs were completely closed anatomically as shown by both ophthalmoscopy and optical coherence tomography. The preoperative median BCVA was 20/100 (range, 20/200 to 20/50). The postoperative median BCVA was 20/32 (range, 20/200 to 20/20). Visual acuity improved in 9 eyes (90%) by ≥2 Snellen lines and was unchanged in 1 eye. In two

cases, complications included iatrogenic peripheral retinal breaks, which were treated by endolaser photocoagulation intraoperatively. In only one MH case was there an elevation of IOP (26 mmHg) after 6 months, and this was treated with latanoprost (Xalatan®, Pfizer Japan Inc., Tokyo, Japan) (Table 1).

In ERM cases, the mean foveal thickness of retina ± SD measured by optical coherence tomography decreased from 454.7 ± 141.3 μm (preoperative) to

Fig. 3. Transmission electron micrographs of the removed internal limiting membrane (ILM). The removed ILM shows an irregular surface on the retinal side (R), which is associated with fragments of Müller cells (arrowheads). The vitreous side showed a smooth surface (V). This examination confirmed the presence of the ILM in all processed specimens from four eyes (original magnification, ×2,600).

249.4 ± 71.3 μm (postoperative). Postoperative BCVA (range, 20/100 to 20/12.5; median, 20/32) was better than preoperative BCVA (range, 20/100 to 20/40; median, 20/50) in ERM cases (Table 2). Eight patients (80%) had an improvement of ≥2 Snellen lines, whereas BCVA remained the same or improved by 1 line for the other two patients. The only complication was the protraction of vitreous hemorrhage in one case, which was absorbed after observation. No other adverse effects such as retinal pigment epithelium atrophy were observed during the follow-up period in all cases.

Discussion

The application of dyes such as ICG and TB has enabled surgeons to perform ILM and ERM peeling procedures with improved ease.[1-6] However, the adverse effects of these dyes on the retina have been widely reported.[7-16] Furthermore, there have been several recent reports demonstrating that the damage to retinal cells by ICG and TB causes apoptotic cell death.[24,25]

In the present study, a low dose of BBG (0.25 mg/mL) was found to selectively stain the ILM safely and with ease. The staining mechanism of BBG at the ILM still remains unknown. To our knowledge, this clinical study is the first report of the ophthalmic use of BBG in humans. Seventeen patients (85%) had visual acuity improved by at least 2 Snellen lines, and no adverse effects were observed postoperatively during the observation period.

BBG is a blue dye (color index 42655) with the formula $C_{47}H_{48}N_3O_7S_2Na$ (molecular weight, 854.0) that is also known as acid blue 90 and Coomassie BBG. BBG has been used for protein staining in biologic fields, because it binds nonspecifically to virtually all proteins. It is also used as a protein electrophoresis dye. The pharmacological function of BBG still remains unconfirmed. However, although there are no reports on the medical use of this dye, there is a long history of biologic use in which no apparent toxicity has been reported. Before this study, we examined the effects of intravitreal BBG on the morphology and functions of the retina in rat eyes and continued the investigation to examine the possible use of BBG for ILM staining and ILM peeling in primate eyes, because BBG is for experimental use only at present. In the rat eyes, no apparent pathologic changes were observed in all dose groups (from 0.01 mg/mL to 10 mg/mL) by light microscopy. Although electron microscopy showed cyst formation in the inner retinal cells in high-dose groups (1.0 mg/mL and 10 mg/mL), the apparent apoptotic cell death of the

retinal cell was not detected, and the amplitude of electroretinogram waves demonstrated no remarkable reduction after both 14 days and 2 months. In the primate eyes, the ILM was clearly visualized after the intravitreous injection of 0.5 mg/mL BBG.[18]

BBG has a number of advantages over other dyes such as ICG and TB. BBG is easier to handle than both ICG and TB because it is produced in a granular form that can be easily dissolved with intraocular irrigating solution alone and subsequently sterilized with a syringe filter. When compared with saline or intraocular irrigating solution, the osmolarity and pH of the BBG solution are very stable.[17,18] The ILM staining pattern produced by the BBG solution was similar to that produced by the ICG solution. However, because BBG is not a fluorescent dye, there is little possibility of light toxicity such as that produced with ICG. Besides, no additional techniques such as fluid–gas exchange, which TB use requires, are needed for BBG staining.[3,4] Furthermore, the BBG concentrations required for staining the ILM are ≈1/10 to 1/20 lower than those required with ICG. The improvements in visual acuity achieved in this case study using BBG are comparable with those of previous studies using different dyes,[2,4,7,12,15] although it is thought that further safety evaluations of BBG for use in human eyes will be required in the future. Further investigation is necessary before any clinical recommendations can be given. From the results of our preclinical study[17,18] and this clinical study, we conclude that BBG is a potentially useful dye for ILM staining, making BBG-assisted membrane peeling a potentially effective and safe means of managing MH and ERM surgery.

Key words: brilliant blue G, vitrectomy, internal limiting membrane, epiretinal membrane, macular hole, clinical case series.

References

1. Burk SE, Da Mata AP, Snyder ME, et al. Indocyanine green-assisted peeling of the retinal internal limiting membrane. Ophthalmology 2000;107:2010–2014.
2. Kadonosono K, Itoh N, Uchio E, et al. Staining of internal limiting membrane in macular hole surgery. Arch Ophthalmol 2000;118:1116–1118.
3. Feron EJ, Veckeneer M, Parys-Van Ginderdeuren R, et al. Trypan blue staining of epiretinal membranes in proliferative vitreoretinopathy. Arch Ophthalmol 2002;120:141–144.
4. Perrier M, Sebag M. Trypan blue-assisted peeling of the internal limiting membrane during macular hole surgery. Am J Ophthalmol 2003;135:903–905.
5. Gandorfer A, Messmer EM, Ulbig MW, Kampik A. Indocyanine green selectively stains the internal limiting membrane. Am J Ophthalmol 2001;131:387–388.
6. Kusaka S, Hayashi N, Ohji M, et al. Indocyanine green facilitates removal of epiretinal and internal limiting mem-

branes in myopic eyes with retinal detachment. Am J Ophthalmol 2001;131:388–390.

7. Haritoglou C, Eibl K, Schaumberger M, et al. Functional outcome after trypan blue-assisted vitrectomy for macular pucker: a prospective, randomized, comparative trial. Am J Ophthalmol 2004;138:1–5.

8. Enaida H, Sakamoto T, Hisatomi T, et al. Morphological and functional damage of the retina caused by intravitreous indocyanine green in rat eyes. Graefes Arch Clin Exp Ophthalmol 2002;240:209–213.

9. Sippy BD, Engelbrecht NE, Hubbard GB, et al. Indocyanine green effect on cultured human retinal pigment epithelial cells: implication for macular hole surgery. Am J Ophthalmol 2001;132:433–435.

10. Stalmans P, Van Aken EH, Veckeneer M, et al. Toxic effect of indocyanine green on retinal pigment epithelium related to osmotic effects of the solvent. Am J Ophthalmol 2002;134: 282–285.

11. Gandorfer A, Haritoglou C, Gass CA, et al. Indocyanine green-assisted peeling of the internal limiting membrane may cause retinal damage. Am J Ophthalmol 2001;132:431–433.

12. Haritoglou C, Gandorfer A, Gass CA, et al. Indocyanine green-assisted peeling of the internal limiting membrane in macular hole surgery affects visual outcome: a clinicopathologic correlation. Am J Ophthalmol 2002;134:836–841.

13. Uemura A, Kanda S, Sakamoto Y, Kita H. Visual field defects after uneventful vitrectomy for epiretinal membrane with indocyanine green-assisted internal limiting membrane peeling. Am J Ophthalmol 2003;136:252–257.

14. Veckeneer M, van Overdam K, Monzer J, et al. Ocular toxicity study of trypan blue injected into the vitreous cavity of rabbit eyes. Graefes Arch Clin Exp Ophthalmol 2001;239: 698–704.

15. Haritoglou C, Gandorfer A, Schaumberger M, et al. Trypan blue in macular pucker surgery: an evaluation of histology and functional outcome. Retina 2004;24:582–590.

16. Yam HF, Kwok AK, Chan KP, et al. Effect of indocyanine green and illumination on gene expression in human retinal pigment epithelial cells. Invest Ophthalmol Vis Sci 2003;44: 370–377.

17. Hisatomi T, Enaida H, Matsumoto H, et al. The biocompatibility of brilliant blue G: preclinical study of brilliant blue G as an adjunct for capsular staining. Arch Ophthalmol (in press).

18. Enaida H, Hisatomi T, Goto Y, et al. Preclinical investigation of internal limiting membrane peeling and staining using intravitreal brilliant blue G. Retina 2006;26:623–630.

19. Sakamoto T, Miyazaki M, Hisatomi T, et al. Triamcinolone-assisted pars plana vitrectomy improves the surgical procedures and decreases the postoperative blood-ocular barrier breakdown. Graefes Arch Clin Exp Ophthalmol 2002;240: 423–429.

20. Enaida H, Hata Y, Ueno A, et al. Possible benefits of triamcinolone-assisted pars plana vitrectomy for retinal diseases. Retina 2003;23:764–770.

21. Enaida H, Hata Y, Ueno A, et al. Visualization of the Cloquet canal during triamcinolone-assisted vitrectomy. Arch Ophthalmol 2004;122:1564–1565.

22. Weiss JN, Bynoe LA. Injection of tissue plasminogen activator into a branch retinal vein in eyes with central retinal vein occlusion. Ophthalmology 2001;108:2249–2257.

23. Asami T, Terasaki H, Kachi S, et al. Ultrastructure of internal limiting membrane removed during plasmin-assisted vitrectomy from eyes with diabetic macular edema. Ophthalmology 2004;111:231–237.

24. Rezai KA, Farrokh-Siar L, Ernest JT, van Seventer GA. Indocyanine green induces apoptosis in human retinal pigment epithelial cells. Am J Ophthalmol 2004;137:931–933.

25. Rezai KA, Farrokh-Siar L, Gasyna EM, Ernest JT. Trypan blue induces apoptosis in human retinal pigment epithelial cells. Am J Ophthalmol 2004;138:492–495.

Staining Ability and Biocompatibility of Brilliant Blue G

Preclinical Study of Brilliant Blue G as an Adjunct for Capsular Staining

Toshio Hisatomi, MD, PhD; Hiroshi Enaida, MD, PhD; Hiroyoshi Matsumoto, MD; Tadahisa Kagimoto, MD; Akifumi Ueno, MD; Yasuaki Hata, MD, PhD; Toshiaki Kubota, MD, PhD; Yoshinobu Goto, MD, PhD; Tatsuro Ishibashi, MD, PhD

Objective: To evaluate the effectiveness and biocompatibility of brilliant blue G (BBG) for capsular visualization for continuous curvilinear capsulorrhexis.

Methods: The capsular staining ability of BBG was evaluated at graded concentrations of 10.0, 1.0, 0.5, 0.25, 0.1, and 0.01 mg/mL in enucleated pig's eyes. The biocompatibility of BBG was assessed in rat's eyes for 2 months. The eyes were analyzed using light, fluorescence, transmission electron, and scanning electron microscopy. TUNEL (terminal deoxynucleotidyl transferase–mediated biotin–deoxyuridine triphosphate nick-end labeling) was used to detect apoptotic cells, and endothelial cell counts were analyzed using scanning electron microscopy. The results were compared using indocyanine green and trypan blue.

Results: The BBG improved capsular visualization, and a complete capsulorrhexis could be performed. In the rat model, no apparent toxic effect was observed using biomicroscopy during 2 months. Histologically, BBG showed satisfactory biocompatibility. Apoptotic cell death of the endothelial cells was detected in only the trypan blue group. In contrast to BBG, indocyanine green and trypan blue showed degeneration of corneal endothelial cells using transmission and scanning electron microscopy.

Conclusion: The BBG contributed to better capsular visualization and caused no apparent complications to the corneal endothelium.

Clinical Relevance: The BBG is effective and safe capsular staining for continuous curvilinear capsulorrhexis.

Arch Ophthalmol. 2006;124:514-519

C REATING A CONTINUOUS curvilinear capsulorrhexis (CCC) in an eye with a white mature cataract can be challenging because it is difficult to distinguish the anterior capsule from the underlying white cortex. Poor visualization of the capsule tends to result in an incomplete or inadequate CCC, which could cause a subsequent capsular tear, vitreous loss, and intraocular lens dislocation. To alleviate this problem, the intraocular administration of dyes for anterior capsule staining to aid in the performance of CCC in eyes with cataracts in which there is poor or no red reflex has become increasingly popular.[1,2] Dada et al[3] demonstrated that capsular staining facilitates CCC even in immature cataracts and could be a useful adjunct for trainee surgeons. Trypan blue (TB) (0.1% and 0.06%) has already been introduced for capsular staining and has been found to have no apparent toxic effects in vivo.[2-4] However, TB has been reported to be toxic to corneal endothe-

lium in vitro in severe conditions.[5] Another dye, indocyanine green (ICG), is also frequently used for capsular staining.[1,6,7] McEnerney and Peyman[8] described the use of ICG for cell counts in rabbit corneal endothelium and suggested that the dye did not damage living endothelium. However, our group[9] reported the potential toxic effects of ICG to retinal cells in 2002, and recently the toxic effects of ICG have been reported in retinal pigment epithelium, ganglion cells, and photoreceptors.[10,11] Both TB and ICG, therefore, have been shown to have shortcomings regarding capsular staining. What is now sought is an ideal dye, possessing satisfactory staining ability yet with minimal toxic effects, that can be used to facilitate the successful creation of CCC. In the present study, we investigate a new dye, brilliant blue G (BBG), which stains the anterior capsule at a lower concentration than the other dyes in common use while showing minimal toxic effects. This experimental study reports the effectiveness and biocompatibility of BBG in capsular staining.

Author Affiliations: Departments of Ophthalmology (Drs Hisatomi, Enaida, Matsumoto, Kagimoto, Ueno, Hata, and Ishibashi) and Neurophysiology (Dr Goto), Graduate School of Medical Sciences, Kyushu University, and Department of Ophthalmology, University of Occupational and Environmental Health (Dr Kubota), Fukuoka, Japan.

All procedures conformed to the Association for Research in Vision and Ophthalmology statement for the Use of Animals in Ophthalmic and Vision Research and the guidelines for animal care at Kyushu University.

CAPSULAR STAINING ABILITY OF BBG

Pig's eyes were obtained from a local slaughterhouse and transported to the laboratory on ice. The extraocular muscles and other connective tissues were carefully cut off, and the eyes were placed on the operation chamber. Brilliant blue G is a blue dye (color index No. 42655, $C_{47}H_{48}N_3O_7S_2Na$, and molecular weight 854.0) that is also known as acid blue 90 and Coomassie BBG. The dye has been used for protein staining in biological fields because it binds nonspecifically to almost all proteins. The dye is also often used for gel electrophoresis. The pharmacologic function of the dye remains unconfirmed. There are no reports on the medical use of this dye, but there is a long history of biological use in which no apparent toxic effects have been reported. To our knowledge, this is the first article to examine the toxic effects of BBG used for medical and ophthalmic purposes. The BBG solution was prepared using the following method. Twenty milligrams of BBG (Coomassie Brilliant Blue G 250; Sigma-Aldrich Corp, St Louis, Mo) was dissolved in 10 mL of intraocular irrigating solution (Opeguard-MA; Senjyu Pharmaceutical Co Ltd, Osaka, Japan) and sterilized using a syringe filter (Minisart; Sartorius AG, Goettingen, Germany). The capsular staining effected by BBG was then examined under the surgical microscope as follows. The anterior chamber was entered through the clear cornea using a 26-gauge needle mounted on a syringe. The BBG (10, 1, 0.5, 0.25, 0.1, and 0.01 mg/mL) was injected onto the anterior capsule through a 26-gauge needle introduced through the same entry. The anterior chamber was immediately irrigated using enhanced balanced salt solution (BSS) (BSS Plus; Santen Pharmaceutical Co Ltd, Osaka, Japan) so that the excessive dye was easily washed out.

To deepen the anterior chamber, 1% sodium hyaluronate (Healon; Pharmacia, Uppsala, Sweden) was injected. A CCC was initiated by preparing a small triangular anterior capsular flap using a bent 26-gauge disposable needle mounted on a viscoelastic syringe. The CCC was completed using a cystotome or capsulorrhexis forceps.

BIOCOMPATIBILITY OF BBG

Brown Norway rats (Kyudo, Fukuoka), at postnatal 8 week, were studied in the following manner. The rats were anesthetized with an intraperitoneal injection of sodium pentobarbital, and their pupils were dilated with topical 1% tropicamide and 2.5% phenylephrine hydrochloride. The right eye of each rat was examined in the following experiments (N=54). The anterior chamber was entered through the clear cornea using a 30-gauge needle mounted on a syringe, and a single anterior chamber injection was then performed with each dye—BBG (10, 1, 0.5, 0.25, 0.1, and 0.01 mg/mL), ICG (5 mg/mL), and TB (1 mg/mL)—and the control Opeguard-MA solution (n=6 for each). The mean osmolarity of each solution is given in the **Table**. The dye remained in the anterior chamber and was followed by biomicroscopic examination for 2 months. The eyes were enucleated 2 weeks and 2 months after surgery. The right eye of each rat was then examined in the following sequence of experiments (N=54): light microscopy, transmission electron microscopy, and scanning electron microscopy.

Table. Osmolarity of Each Dye Solution

Solution	Concentration, mg/mL	Osmolarity, mOsm/kg H₂O
BBG	10	310
	1	300
	0.5	299
	0.25	298
	0.1	298
	0.01	298
ICG	5	271
TB	1	316
Control (vehicle)	NA	298

Abbreviations: BBG, brilliant blue G; ICG, indocyanine green; NA, not applicable; and TB, trypan blue.

Light Microscopy

The eyes were fixed in 4% paraformaldehyde and cut in half, embedded in paraffin, deparaffinized in xylene, rehydrated in ethanol, and washed in phosphate-buffered saline (PBS). The 4-μm-thick sections were stained by hematoxylin-eosin and observed by light microscopy (3 per dye, a total of 27 eyes).

Terminal Deoxynucleotidyl Transferase–Mediated Biotin–Deoxyuridine Triphosphate Nick-End Labeling

TUNEL (terminal deoxynucleotidyl transferase–mediated biotin-deoxyuridine triphosphate nick-end labeling) was used to detect apoptotic cell death.[12,13] Four-micron-thick sections were made from samples fixed in 4% paraformaldehyde and embedded in paraffin. The TUNEL staining was performed on these sections using a fluorescein direct in situ apoptosis detection kit (ApopTag; Intergen Co, New York, NY) according to the manufacturer's protocols. The sections were then co-stained with propidium iodide (Molecular Probes, Eugene, Ore), thus allowing observation of the cell nuclei by using a fluorescence microscope (Olympus, Tokyo, Japan). Ten sections for each eye specimen were randomly selected and observed (3 per dye, a total of 27 eyes).

Transmission Electron Microscopy

Enucleated eyes and their anterior segments were fixed in 1% glutaraldehyde and 1% paraformaldehyde in PBS (3 per dye, a total of 27 eyes). The anterior segment was then cut in half. The specimens were postfixed in veronal acetate buffer osmium tetroxide (2%), dehydrated in ethanol and water, and embedded in Epon. From these, ultrathin sections were cut and mounted on copper grids. The specimens were observed by using an electron microscope (JEM-100CX; JEOL, Tokyo).[12,13]

Scanning Electron Microscopy

Enucleated eyes and their anterior segments were fixed in 1% glutaraldehyde and 1% paraformaldehyde in PBS (3 per dye, a total of 27 eyes). The anterior segment was then cut in half. The specimens were postfixed in veronal acetate buffer osmium tetroxide (2%) and dehydrated in ethanol and water. The specimens were then saturated in t-butyl alcohol and dried using a critical point dryer (Eiko, Tokyo). The specimens were then placed on stubs by means of self-adhering carbon tabs and were sputtered with 20-nm-thick gold using an argon plasma
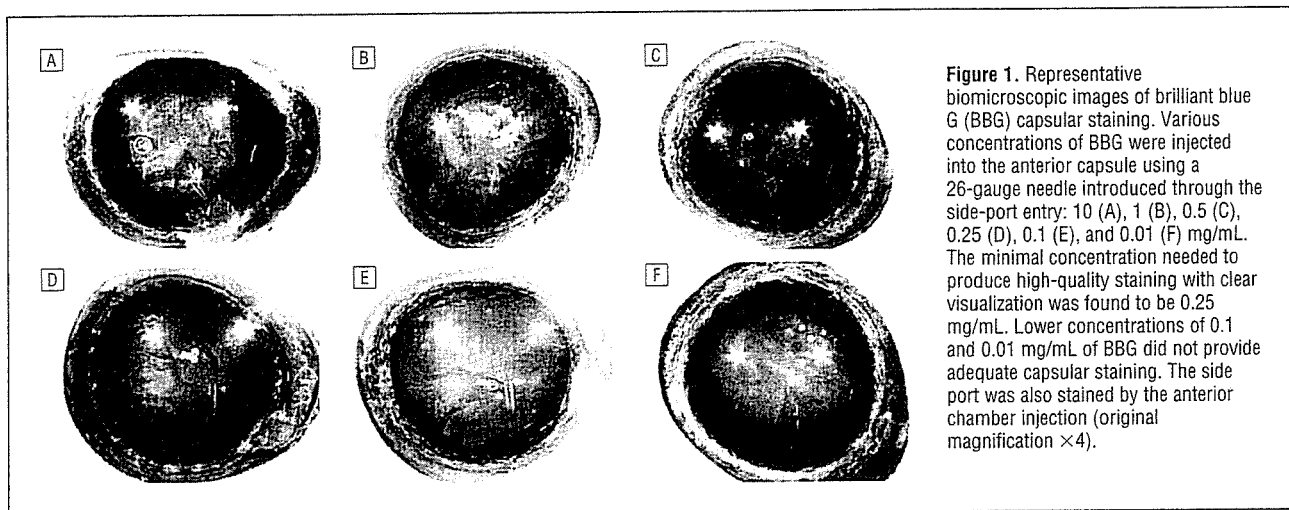
Figure 1. Representative biomicroscopic images of brilliant blue G (BBG) capsular staining. Various concentrations of BBG were injected into the anterior capsule using a 26-gauge needle introduced through the side-port entry: 10 (A), 1 (B), 0.5 (C), 0.25 (D), 0.1 (E), and 0.01 (F) mg/mL. The minimal concentration needed to produce high-quality staining with clear visualization was found to be 0.25 mg/mL. Lower concentrations of 0.1 and 0.01 mg/mL of BBG did not provide adequate capsular staining. The side port was also stained by the anterior chamber injection (original magnification ×4).

coater (Eiko). Finally, the endothelial surface of the cornea was studied using a scanning electron microscope (JEM-840; JEOL).[14,15] A 1-mm^2 area was analyzed using scanning electron microscopy to find the endothelial cell count, the results of which are given as mean±SD (3 per dye).

RESULTS

CAPSULAR STAINING BY BBG

The capsular staining ability of BBG was assessed in pig's eyes using graded concentrations of the dye. The dye stained the anterior capsule homogenously, and the edge of the CCC could be clearly observed under the surgical microscope. The staining deepened as the concentration of the dye increased (from 0.25 to 1 mg/mL) (**Figure 1**), and the minimal concentration needed to produce high-quality staining with clear visualization was found to be 0.25 mg/mL (Figure 1). At 0.1 and 0.01 mg/mL, the capsular staining was obscure, and no merit could be found in using the dye (Figure 1). The side port was also stained by the anterior chamber injection.

BIOCOMPATIBILITY OF BBG

Light Microscopy

Sections of the cornea stained with hematoxylin-eosin showed no remarkable changes in any group (BBG, ICG, and TB) (data not shown). In the light microscopic examination, no signs of endothelial cell loss or corneal edema were observed. The lamellar collagen layers, stromal cells, and epithelial cell layer were well preserved. No inflammatory cell infiltration was observed in any corneal layers.

Apoptotic Cell Death Detected Using TUNEL

In all the groups, apoptotic cell death of the corneal epithelium due to physiologic turnover was observed occasionally (**Figure 2**). In the BBG groups, no TUNEL staining was observed in the corneal stromal cells, endothelium, ciliary body, and lens cells (Figure 2). In the ICG group,

no apparent apoptotic cell death was detected in the 5-mg/mL concentration. In the TB group, apoptotic cell death of the corneal endothelium was detected in 2% of all endothelial cells. The other cells in the TB group did not undergo apoptotic cell death.

Transmission Electron Microscopy

In the BBG groups, the ultrastructure of the corneal cells and collagen cellular matrix was well preserved in the highest concentration (10 mg/mL) (**Figure 3**). In the corneal endothelium, cellular membranes, well-defined nuclei, and cytoplasmic organella showed no degenerative changes (Figure 3). The ICG group showed well-preserved structure of endothelial cells, but some endothelial cells demonstrated signs of mitochondrial swelling (Figure 3). The TB group showed cyst formation in the endothelial cell layer due to separation between the cells and occasional degeneration of the corneal endothelium in a patchy manner (Figure 3).

Scanning Electron Microscopy

In the BBG-exposed corneas, scanning electron microscopy showed normal cells similar to those in the controls. The scanning electron microscopic image demonstrated a normal hexagonal endothelial cell sheet with intact borders and no endothelial swelling (**Figure 4**). The ICG group also showed some cellular swelling in the corneal endothelial sheet. Occasionally, degenerated endothelial cells were observed to have broken free from their original location. In the TB group, endothelial cell shrinkage was recognized in the central area of the cornea, which led to endothelial cell loss in a sporadic manner. The mean corneal endothelial cell counts were 7728±268/mm^2 in the control group, 7642±317/mm^2 in the BBG groups, 7501±230/mm^2 in the ICG group, and 7030±246/mm^2 in the TB group.

COMMENT

To our knowledge, this is the first study of staining by the new dye BBG. Many dyes have previously been

examined for their staining ability of the anterior capsule and toxic effects in vitro and in vivo.[1,2,6] However few have been used to stain the anterior capsule in human eyes. Those used to date include TB,[2] ICG,[1] gentian violet,[16] fluorescein,[17] and methylene blue. These dyes can be used to stain the capsule from above, under an air bubble,[1,2,18] or by intracameral subcapsular injection,[17-19] and ICG and TB are now commonly used to stain the anterior capsule with no apparent toxic effects under normal conditions. Nevertheless, we demonstrate that BBG has better staining ability and biocompatibility than either ICG or TB.

STAINING ABILITY AND EASE OF HANDLING OF BBG

In the present study, BBG revealed positive blue staining of the anterior capsule, providing a striking contrast to the white lens cortex and red retinal reflex. Under the surgical microscope, BBG blue staining provided a better contrast than ICG green and TB blue staining. In addition, satisfactory staining was obtained at the lower concentration of 0.25 mg/mL of BBG compared with 5 mg/mL of ICG and 1 mg/mL of TB.[2]

In terms of handling, BBG also has advantages over ICG and TB. Indocyanine green is packaged as lyophilized powder and will not dissolve properly in BSS alone; ICG first has to be diluted in 0.5 mL of aqueous solvent before adding 4.5 mL of BSS. Furthermore, if the aqueous solvent, namely, the distilled water vehicle, is injected into the anterior chamber without being diluted with BSS, corneal edema can result with or without ICG. In addition, in practical terms, all reconstituted ICG must be used on the same day, and it is more expensive than the alternative dye (TB). In contrast, TB can easily be diluted in BSS, although, owing to its low affinity to the anterior capsule, it is beneficial to undertake fluid-air exchange of the anterior chamber before effecting capsular staining. Thus, after air injection into the anterior chamber, TB can be injected drop by drop under the air bubble.[3,4] On the other hand, BBG was easily diluted in BSS alone, and satisfactory capsular staining was obtained by a single injection into the anterior chamber without the need for fluid-air exchange. The capsular staining was obtained immediately after the injection, and the excessive dye was easily washed out with BSS irrigation.

Thus, the results of this study show that BBG has effective staining ability combined with ease of handling. Brilliant blue G provided better staining at lower concentrations than either ICG or TB in a clinically relevant model for the study of capsular staining in pig's eyes. The minimal concentration of BBG needed to demonstrate favorable staining with clear visualization was 0.25 mg/mL. Furthermore, BBG could easily be dissolved directly in the irrigation solution.

BIOCOMPATIBILITY OF BBG

Indocyanine green has been reported to possess good biocompatibility with the anterior chamber when injected under normal conditions. However, it has also been reported that the intravitreous injection of ICG could cause
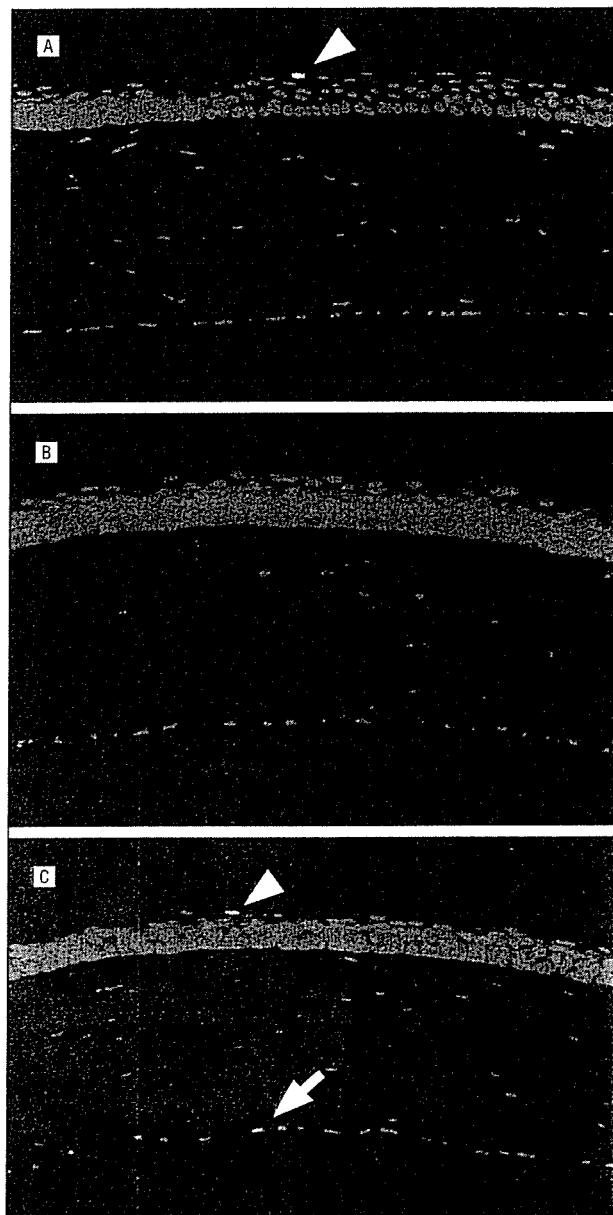

Figure 2. Apoptotic cell death detected by TUNEL (terminal deoxynucleotidyl transferase–mediated biotin–deoxyuridine triphosphate nick-end labeling). In all the groups, apoptotic cell death of the corneal epithelium due to physiologic turnover was observed occasionally. A, In the brilliant blue G groups, no TUNEL staining was observed in the corneal stromal cells or in the endothelium. Arrowhead indicates apoptotic epithelial cell. B, In the indocyanine green group, no apparent apoptotic cell death was detected at the 5-mg/mL concentration. C, In the trypan blue group, apoptotic cell death of the corneal endothelium was detected in endothelial cells (original magnification ×400). Arrow indicates apoptotic endothelial cell; arrowhead, apoptotic epithelial cell.

retinal degeneration.[9] In addition, ICG has recently been reported to cause retinal pigment epithelial atrophy,[11,20-22] photoreceptor apoptosis,[23] glial cells,[11] and retinal ganglion cell loss.[24] The adverse clinical effects of visual field loss, possibly related to the use of ICG in vitrectomy, have also been reported.[25,26] In severe conditions, our rat experimental model showed that ICG also caused swelling of the cytoplasmic organella (mitochondria) and cellular degeneration. Trypan blue has a long history of safety in ophthalmologic use.[4,8,27-29] Some de-
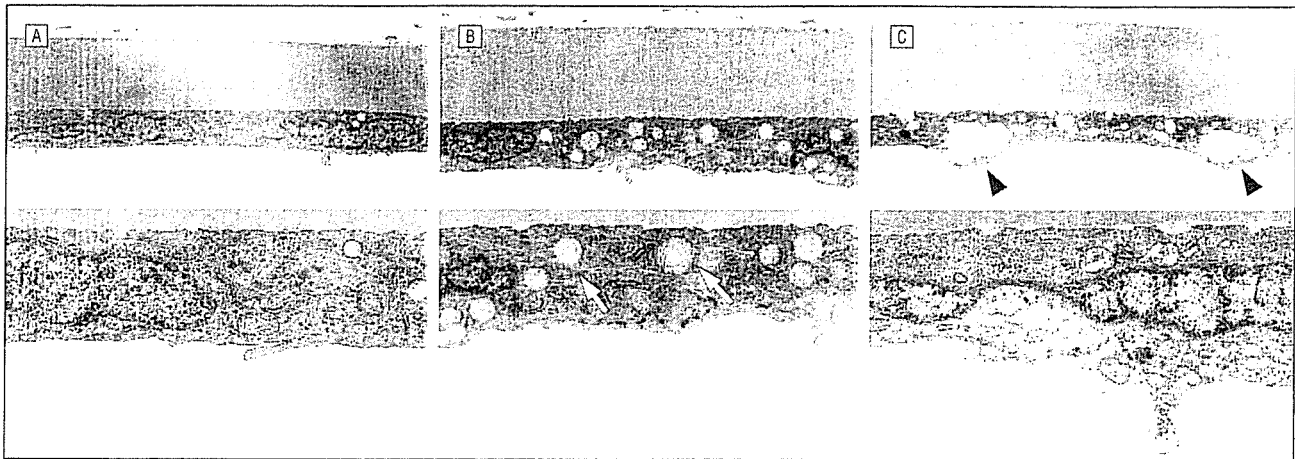
Figure 3. Ultrastructure of the corneal cells studied using transmission electron microscopy. A, In the brilliant blue G groups, the ultrastructure of the corneal cells and collagen cellular matrix was well preserved at the highest concentration (10 mg/mL). B, The indocyanine green group showed mitochondrial swelling at the 5-mg/mL concentration (arrows). C, The trypan blue group showed cyst formation in the endothelial cell layer due to separation of the cells and degeneration of the corneal endothelium in a sporadic manner (arrowheads) (top: original magnification ×3300; bottom: original magnification ×6600).
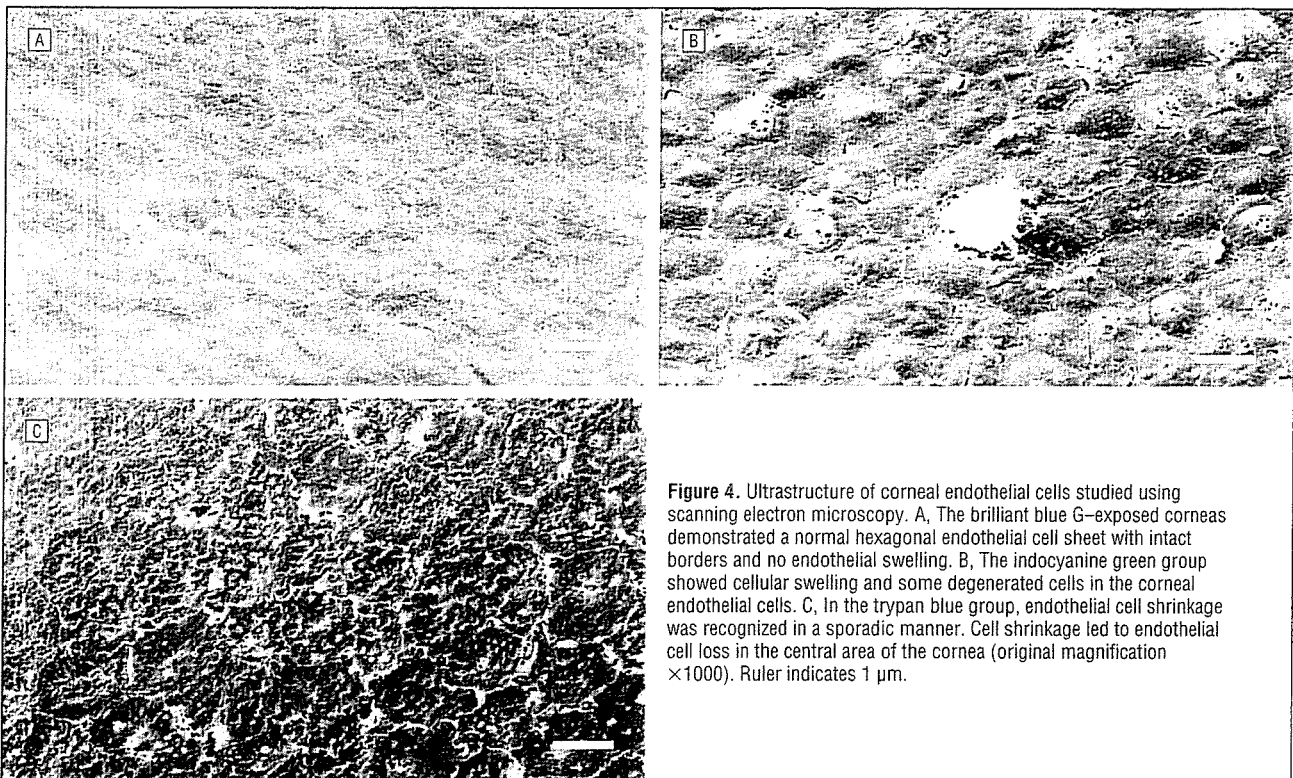
Figure 4. Ultrastructure of corneal endothelial cells studied using scanning electron microscopy. A, The brilliant blue G–exposed corneas demonstrated a normal hexagonal endothelial cell sheet with intact borders and no endothelial swelling. B, The indocyanine green group showed cellular swelling and some degenerated cells in the corneal endothelial cells. C, In the trypan blue group, endothelial cell shrinkage was recognized in a sporadic manner. Cell shrinkage led to endothelial cell loss in the central area of the cornea (original magnification ×1000). Ruler indicates 1 μm.

tailed examinations have reported fewer toxic effects of TB than ICG in glial cells and retinal pigment epithelium cell cultures.[11,20] However, TB has also been reported to possess potential toxicity when introduced into cultured retinal pigment epithelium.[30] In the present study, scanning electron microscopy showed corneal endothelial shrinkage in a sporadic manner as a result of the injection of TB into the anterior chamber. This could be due to the toxicity of TB or to the high osmolarity of the TB solution. Although some previous studies[4,31] reported on the safety of ICG and TB in endothelial cells, under the more severe experimental conditions of the present study, the potential toxicity of the dyes was re-

vealed. In contrast to ICG and TB, the anterior chamber injection of BBG showed no remarkable toxic effects histologically, even at 10 mg/mL. Functionally, the cornea did not show edema, and it remained transparent throughout the observation period. Apoptotic cell death observed by TUNEL also confirmed the lower toxicity of BBG compared with TB. With high affinity and biocompatibility with the anterior chamber, BBG is, therefore, a good candidate for a capsular staining dye.

The osmolarity of the solution is an important factor for the toxicity for cell survival.[32] We, therefore, tested the osmolarity of each solution (Table 1). Indocyanine green has a much lower osmolarity than the control be-

cause of the aqueous solvent used in the dilution, whereas the osmolarity of TB is higher than that of the control. In contrast, BBG (0.25 mg/mL) has an almost identical osmolarity to the control.

The mean corneal endothelial cell counts were $7728 \pm 268/\text{mm}^2$ in the control group, $7642 \pm 317/\text{mm}^2$ in the BBG groups, $7501 \pm 230/\text{mm}^2$ in the ICG group, and $7030 \pm 246/\text{mm}^2$ in the TB group. Thus, although BBG showed marginally less toxicity, there was no significant difference across the 4 groups. In rat's eyes, corneal endothelial cells are known to have a higher proliferative capacity than in human endothelial cells. Our endothelial cell count of rat's eyes is suggestive for clinical use; however, the data do not apply to human endothelial cell counts. Although the corneal endothelial cell count did not change in the observation period in the present study, further research is now needed in human clinical studies.

In conclusion, the results of this study show high biocompatibility of BBG for use in capsular staining. Brilliant blue G demonstrated better-preserved morphologic features of corneal endothelial cells using transmission and scanning electron microscopy than ICG and TB. Also, TUNEL confirmed the lower toxicity of BBG vs TB. Because rat corneal endothelial cells have higher proliferative capacity than human endothelial cells, the rat data do not apply to human eyes, and further detailed studies are needed in human clinical studies. In addition, the BBG solution has an osmolarity similar to that of the physiologic aqueous humor. Thus, BBG is a good alternative dye for capsular staining, with superior staining ability and biocompatibility.

REFERENCES

1. Horiguchi M, Miyake K, Ohta I, Ito Y. Staining of the lens capsule for circular continuous capsulorrhexis in eyes with white cataract. *Arch Ophthalmol.* 1998; 116:535-537.
2. Melles GR, de Waard PW, Pameyer JH, Houdijn Beekhuis W. Trypan blue capsule staining to visualize the capsulorhexis in cataract surgery. *J Cataract Refract Surg.* 1999;25:7-9.
3. Dada T, Ray M, Bhartiya P, Vajpayee RB. Trypan-blue–assisted capsulorhexis for trainee phacoemulsification surgeons [letter]. *J Cataract Refract Surg.* 2002; 28:575-576.
4. van Dooren BT, de Waard PW, Poort-van Nouhuys H, Beekhuis WH, Melles GR. Corneal endothelial cell density after trypan blue capsule staining in cataract surgery [letter]. *J Cataract Refract Surg.* 2002;28:574-575.
5. van Dooren BT, Beekhuis WH, Pels E. Biocompatibility of trypan blue with human corneal cells. *Arch Ophthalmol.* 2004;122:736-742.
6. Newsom TH, Oetting TA. Indocyanine green staining in traumatic cataract. *J Cataract Refract Surg.* 2000;26:1691-1693.
7. Kobayashi A, Segawa Y, Nishimura A, Shirao Y, Sugiyama K. Indocyanine green staining for the triple corneal procedure. *Ophthalmic Surg Lasers Imaging.* 2004; 35:23-25.
8. McEnerney JK, Peyman GA. Indocyanine green: a new vital stain for use before penetrating keratoplasty. *Arch Ophthalmol.* 1978;96:1445-1447.
9. Enaida H, Sakamoto T, Hisatomi T, Goto Y, Ishibashi T. Morphological and functional damage of the retina caused by intravitreous indocyanine green in rat eyes. *Graefes Arch Clin Exp Ophthalmol.* 2002;240:209-213.
10. Lee JE, Yoon TJ, Oum BS, Lee JS, Choi HY. Toxicity of indocyanine green injected into the subretinal space: subretinal toxicity of indocyanine green. *Retina.* 2003;23:675-681.
11. Jackson TL, Hillenkamp J, Knight BC, et al. Safety testing of indocyanine green and trypan blue using retinal pigment epithelium and glial cell cultures. *Invest Ophthalmol Vis Sci.* 2004;45:2778-2785.
12. Hisatomi T, Sakamoto T, Murata T, et al. Relocalization of apoptosis-inducing factor in photoreceptor apoptosis induced by retinal detachment in vivo. *Am J Pathol.* 2001;158:1271-1278.
13. Hisatomi T, Sakamoto T, Goto Y, et al. Critical role of photoreceptor apoptosis in functional damage after retinal detachment. *Curr Eye Res.* 2002;24:161-172.
14. Hisatomi T, Sakamoto T, Sonoda KH, et al. Clearance of apoptotic photoreceptors: elimination of apoptotic debris into the subretinal space and macrophage-mediated phagocytosis via phosphatidylserine receptor and integrin alphavbeta3. *Am J Pathol.* 2003;162:1869-1879.
15. Hisatomi T, Enaida H, Sakamoto T, et al. A new method for comprehensive bird's-eye analysis of the surgically excised internal limiting membrane. *Am J Ophthalmol.* 2005;139:1121-1122.
16. Unlu K, Aksunger A, Soker S, Ertem M. Mitomycin C primary trabeculectomy with releasable sutures in primary glaucoma. *Jpn J Ophthalmol.* 2000;44:524-529.
17. Fritz WL. Fluorescein blue, light-assisted capsulorhexis for mature or hypermature cataract. *J Cataract Refract Surg.* 1998;24:19-20.
18. Pandey SK, Werner L, Escobar-Gomez M, Roig-Melo EA, Apple DJ. Dye-enhanced cataract surgery, part 1: anterior capsule staining for capsulorhexis in advanced/white cataract. *J Cataract Refract Surg.* 2000;26:1052-1059.
19. Hoffer KJ, McFarland JE. Intracameral subcapsular fluorescein staining for improved visualization during capsulorhexis in mature cataracts [letter]. *J Cataract Refract Surg.* 1993;19:566.
20. Gale JS, Proulx AA, Gonder JR, Mao AJ, Hutnik CM. Comparison of the in vitro toxicity of indocyanine green to that of trypan blue in human retinal pigment epithelium cell cultures. *Am J Ophthalmol.* 2004;138:64-69.
21. Sippy BD, Engelbrecht NE, Hubbard GB, et al. Indocyanine green effect on cultured human retinal pigment epithelial cells: implication for macular hole surgery. *Am J Ophthalmol.* 2001;132:433-435.
22. Engelbrecht NE, Freeman J, Sternberg P Jr, et al. Retinal pigment epithelial changes after macular hole surgery with indocyanine green–assisted internal limiting membrane peeling. *Am J Ophthalmol.* 2002;133:89-94.
23. Kawaji T, Hirata A, Inomata Y, Koga T, Tanihara H. Morphological damage in rabbit retina caused by subretinal injection of indocyanine green. *Graefes Arch Clin Exp Ophthalmol.* 2004;242:158-164.
24. Iriyama A, Uchida S, Yanagi Y, et al. Effects of indocyanine green on retinal ganglion cells. *Invest Ophthalmol Vis Sci.* 2004;45:943-947.
25. Haritoglou C, Gandorfer A, Gass CA, Schaumberger M, Ulbig MW, Kampik A. Indocyanine green–assisted peeling of the internal limiting membrane in macular hole surgery affects visual outcome: a clinicopathologic correlation. *Am J Ophthalmol.* 2002;134:836-841.
26. Gass CA, Haritoglou C, Schaumberger M, Kampik A. Functional outcome of macular hole surgery with and without indocyanine green–assisted peeling of the internal limiting membrane. *Graefes Arch Clin Exp Ophthalmol.* 2003;241:716-720.
27. Sharma N, Bhartiya P, Sinha R, Vajpayee RB. Trypan blue assisted phacoemulsification by residents in training [letter]. *Clin Experiment Ophthalmol.* 2002; 30:386-387.
28. Sperling S. Evaluation of the endothelium of human donor corneas by induced dilation of intercellular spaces and trypan blue. *Graefes Arch Clin Exp Ophthalmol.* 1986;224:428-434.
29. Jacob S, Agarwal A, Agarwal S, Chowdhary S, Chowdhary R, Bagmar AA. Trypan blue as an adjunct for safe phacoemulsification in eyes with white cataract. *J Cataract Refract Surg.* 2002;28:1819-1825.
30. Rezai KA, Farrokh-Siar L, Gasyna EM, Ernest JT. Trypan blue induces apoptosis in human retinal pigment epithelial cells. *Am J Ophthalmol.* 2004;138:492-495.
31. Holley GP, Alam A, Kiri A, Edelhauser HF. Effect of indocyanine green intraocular stain on human and rabbit corneal endothelial structure and viability: an in vitro study. *J Cataract Refract Surg.* 2002;28:1027-1033.
32. Stalmans P, Van Aken EH, Veckeneer M, Feron EJ, Stalmans I. Toxic effect of indocyanine green on retinal pigment epithelium related to osmotic effects of the solvent. *Am J Ophthalmol.* 2002;134:282-285.

Cellular Migration Associated With Macular Hole

A New Method for Comprehensive Bird's-Eye Analysis of the Internal Limiting Membrane

Toshio Hisatomi, MD, PhD; Hiroshi Enaida, MD, PhD; Taiji Sakamoto, MD, PhD; Takaaki Kanemaru, MD; Tadahisa Kagimoto, MD; Ichiro Yamanaka, MD, PhD; Akifumi Ueno, MD; Takao Nakamura, MD, PhD; Yasuaki Hata, MD, PhD; Tatsuro Ishibashi, MD, PhD

Objective: To elucidate the pathogenesis of macular hole formation, focusing in particular on the possible role of cellular migration on the cortical vitreous and internal limiting membrane (ILM) around the macular hole.

Methods: To gain a comprehensive overview of the ILM excised in macular hole surgery (n=36), the ILMs were carefully unfolded and spread out onto glass slides as continuous flat sheets that each contained a macular hole. The specimens were observed by light microscopy and transmission electron microscopy (n=9), and the cellular distribution was analyzed by scanning electron microscopy in a quantitative manner (n=27). Immunohistochemistry for glial fibrillary acidic protein and cytokeratin 18 was carried out for cellular characterization. Cellular proliferation was assessed by immunohistochemistry for proliferating cell nuclear antigen and Ki-67.

Results: Cellular migration was not apparent around the macular hole in the early stage of development of the macular hole (stage 2, 0 μm). As the macular hole passed through the later stages of development, cellular migration developed around the macular hole (stage 3, 84 μm) and the area of cellular migration gradually enlarged (stage 4, 420 μm). The immunophenotypic analysis showed that these cells were mainly glial fibrillary acidic protein–positive glial cells and cytokeratin 18–positive retinal pigment epithelial cells. The proliferating cell nuclear antigen and Ki-67 immunohistochemistry showed that some of these cells were proliferating on the ILM.

Conclusions: Cellular migration on the ILM is not necessary for the initial formation of a macular break. Cellular migration developed after the macular break occurred, and the migration and proliferation increased gradually from the macular hole.

Clinical Relevance: This study provides a new method for understanding the ultrastructural analysis of the pathogenesis of the macular hole.

Arch Ophthalmol. 2006;124:1005-1011

Author Affiliations:
Department of Ophthalmology (Drs Hisatomi, Enaida, Kagimoto, Yamanaka, Ueno, Nakamura, Hata, and Ishibashi) and Morphology Core (Dr Kanemaru), Graduate School of Medical Sciences, Kyushu University, Fukuoka, and Department of Ophthalmology, Kagoshima University School of Medicine, Kagoshima (Dr Sakamoto), Japan.

THE PATHOGENESIS OF THE IDiopathic macular hole is still not fully understood; however, there is agreement on the important role of vitreous attachment and vitreous traction to the underlying internal limiting membrane (ILM) and the retina in the developmental process of the macular hole. Avila et al[1] and Kakehashi et al[2] proposed that anteroposterior traction in the vitreous can cause a macular break. It was suggested that contraction of the prefoveal vitreous cortex might cause tangential traction leading to a macular tear.[3-6] It was also suggested that the premacular vitreous cortex is the posterior wall of the vitreous pocket and that anterior traction by premacular vitreous cortex would lead to intraretinal cyst formation at the fovea following macular hole formation.[7-9] In recent years, ultrasonography,[10,11] confocal laser tomography,[12-14] and optical coherence tomography[15-21] have provided high-resolution cross-sectional images of the retina and vitreous in vivo. Gass[3,5] proposed a classification for the development of a macular hole according to 4 stages. Stage 1 is characterized by focal retinal detachment, stage 2 by early hole formation, stage 3 by a fully developed macular hole without posterior vitreous detachment (PVD), and stage 4 by a macular hole with PVD.

Cellular migration is hypothesized to be one of the major causes of contraction of extracellular matrix such as vitreous cortex.[22-24] Some biomicroscopical studies and histological examinations of surgical and postmortem specimens have identified premacular tissue that may cause tangential traction to the retina.[22,25-27] In addition, histological examinations of excised ILMs demonstrated that migrating cells of various origins were located on the ILM and that these cells were associated with collagen fi-

Specimen No.	Macular Hole Stage	Fixation	Immunohistochemistry†	Hematoxylin-Eosin Staining†	Distance of Cellular Migration From Macular Hole, μm
1	2	PFA	...	‡	0
2	2	GA	...	...	0
3	2	GA	...	...	0
4	2	GA	...	...	0
5	2	PFA	GFAP, CK18	...	0
6	3	GA	...	...	0
7	3	GA	...	...	NA
8	3	GA	...	...	0
9	3	GA	...	...	0
10	3	GA	...	...	0
11	3	GA	...	...	0
12	3	PFA	...	...	NA
13	3	PFA	GFAP, CK18	...	224
14	3	GA	...	...	0
15	3	PFA	GFAP, CK18	...	451
16	4	GA	...	...	359
17	4	GA	...	...	NA
18	4	GA	...	...	0
19	4	GA	...	...	93
20	4	PFA	...	...	NA
21	4	PFA	...	‡	810
22	4	GA	...	...	0
23	4	PFA	Ki-67	...	1210
24	4	PFA	GFAP, CK18	...	850
25	4	PFA	Ki-67	...	320
26	4	PFA	PCNA	...	390
27	4	PFA	PCNA	...	138

Abbreviations: CK18, cytokeratin 18; GA, glutaraldehyde; GFAP, glial fibrillary acidic protein; NA, not applicable; PCNA, proliferating cell nuclear antigen; PFA, paraformaldehyde.

*Twenty-seven specimens were confirmed as stage 2 in 5 eyes, stage 3 in 10 eyes, and stage 4 in 12 eyes. Successful expansion of the folded internal limiting membrane was obtained in 23 specimens, and immunohistochemistry and hematoxylin-eosin staining were carried out in 8 and 2 specimens, respectively.
†Ellipses indicate that the specimens were not analyzed by the method.
‡Specimen was analyzed by hematoxylin-eosin staining.

bers of various diameters.[26-28] Other histological studies[22,25,29] examining postmortem eyes with macular holes noted a high incidence of epiretinal formation in the macular area of the eyes. However, their detailed pathogenesis, especially the role and involvement of cellular migration on the ILM, still remains unclear.

We propose a new method for a topographic bird's-eye analysis of the whole excised ILM. In this study, we describe detailed structures of the ILM around the idiopathic macular hole, the complex association of migrating and proliferating cells, and the extracellular matrix conferred by the developing stages of the macular hole. We examine the characterization and the proliferation of the distributing cells around the macular hole on the ILM.

METHODS

ILM PEELING PROCEDURE

Thirty-nine eyes of 38 patients who were diagnosed as having various stages of the idiopathic macular hole were prospectively studied clinically from January 2002 to July 2004. Biomicroscopical analysis of both the macular and vitreomacular relationships was carried out to identify the macular hole, and each was then graded according to the classification developed by Gass.[3,5,30] A high-resolution optical coherence tomographic examination was used to confirm the state of PVD in each case. The stages of development of the macular holes were confirmed as stage 2 in 8 eyes, stage 3 in 13 eyes, and stage 4 in 15 eyes (total, 36 eyes). All of the data accumulation was carried out with approval from the ethics committee of Kyushu University, Fukuoka, Japan, and was performed in accordance with ethical standards in the 1989 Declaration of Helsinki. After informed consent was obtained from each patient, the patients underwent a standard 3-port pars plana vitrectomy. Balanced salt solution (BSS Plus; Alcon Laboratories, Fort Worth, Tex) was used as an irrigation solution. Triamcinolone acetonide (Kenacolt-A; Bristol Pharmaceuticals KK, Tokyo, Japan), a water-insoluble white corticosteroid, was used for visualizing the vitreous hyaloid as previously described[31-34] (in a 1.0-mL triamcinolone acetonide suspension). If necessary, posterior hyaloid detachment was induced by suction or forceps around the optic nerve head. The vitreous was removed and PVD was extended to the periphery. The ILM was then peeled off with ILM forceps intended to be 3 disc diameters surrounding the macular hole, and fluid-gas exchange was performed through an extrusion cannula over the optic nerve head and macular hole. Twenty-percent sulfahexafluoride gas was then injected after closure of the scleral incisions. Postoperatively, patients were asked to keep a face-down position for at least 5 days.

TRANSMISSION ELECTRON MICROSCOPY OF THE EXCISED ILM

To carry out transmission electron microscopy, the 12 excised specimens (stage 2 in 4 eyes, stage 3 in 4 eyes, and stage 4 in 4 eyes) were immediately placed in 4% glutaraldehyde for fixation. Of the 12 specimens, 9 of them (stage 2 in 3 eyes, stage 3 in 3 eyes, and stage 4 in 3 eyes) were then postfixed in 2% veronal acetate buffer osmium tetroxide, dehydrated in ethanol and water, and embedded in Epon.[35] Ultrathin sections were cut from blocks and mounted on copper grids. The specimens were observed with a JEM 100CX electron microscope (JEOL, Tokyo). Three specimens were further examined by flat-preparation transmission electron microscopy.

FLAT-PREPARATION TRANSMISSION ELECTRON MICROSCOPY

Three fixed specimens (stage 2 in 1 eye, stage 3 in 1 eye, and stage 4 in 1 eye) were dehydrated in ethanol and water, extracted as flat sheets with fine needles under a biomicroscope equipped with dark-field illumination (Nikon, Tokyo), and placed onto a glass slide. Then, the expanded ILMs were embedded in Epon. Ultrathin sections were cut from blocks and mounted on copper grids. The specimens were observed with a JEM 100CX electron microscope.

FLAT PREPARATION FOR COMPREHENSIVE BIRD'S-EYE ANALYSIS OF THE ILM

For scanning electron microscopy, 27 specimens were processed. Fifteen of the excised specimens were fixed in 4% glutaraldehyde. Twelve of the specimens were fixed in 4% paraformaldehyde for light microscopy and immunohistochemistry and then were analyzed by scanning electron microscopy. The fixed ILM was extracted as a flat sheet with fine needles under a biomicroscope equipped with dark-field illumination (Nikon) and placed onto a glass slide. When at least one fourth of the complete macular hole was clearly recognized on the expanded ILM (n=23; 4 specimens were excluded from the total of 27 specimens; **Table**), immunochemistry, scanning electron microscopy, and cellular distribution studies were carried out. Two specimens were stained by hematoxylin-eosin and observed by light microscopy.

IMMUNOHISTOCHEMISTRY OF THE EXPANDED ILM

The ILMs were fixed in 4% paraformaldehyde in phosphate-buffered saline, extracted as whole sheets, and placed onto a glass slide (n=8). The specimens were air dried. The first antibodies against glial fibrillary acidic protein (Dako, Tokyo) (n=4), cytokeratin 18 (Chemicon, Temecula, Calif) (n=4), proliferating cell nuclear antigen (PCNA) (Chemicon) (n=2), and Ki-67 (Dako) (n=2) were used for 2 hours at room temperature. The second antibodies labeled with Cy5 (Zymed Laboratories, San Francisco, Calif) and rhodamine (Cappel, Aurora, Ohio) were used for 1 hour at room temperature. The specimens were also stained with 4',6-diamino-2-phenylindole dihydrochloride for nuclear staining and observed with a fluorescence microscope (Table). The immunohistochemical control experiments included a negative control and an isotype control using the specific IgG subtype. All of the specimens for immunohistochemistry were dehydrated in ethanol and water and then analyzed by scanning electron microscopy.
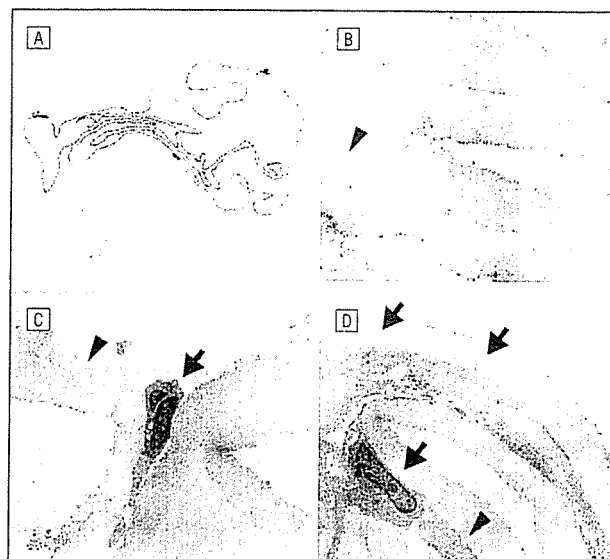

Figure 1. Vertical analysis of the excised internal limiting membrane (ILM). A, Light micrograph of a semithin section of the ILM stained by Azur II, showing characteristic sinusoidal folding (original magnification ×100). B, Transmission electron microscopy showed collagen membranous tissue with a smooth inner (vitreous) surface and an irregular outer (retinal) surface. In the early stage of the macular hole (stage 2), cells were rarely seen. The extracellular matrix, namely, posterior vitreous hyaloid, was seen on the excised ILM intermingled with the distributed cells (arrowhead) (original magnification ×2000). C, Some migrating cells (arrow) were seen on the inner surface of the ILM in stage 3 of development of the macular hole. Again, the extracellular matrix, namely, posterior vitreous hyaloid, was seen on the excised ILM intermingled with the distributed cells (arrowhead) (original magnification ×2000). D, In the later stage (stage 4), significant cellular migration (arrows) was observed on the ILM. The extracellular matrix, namely, posterior vitreous hyaloid, was seen on the excised ILM intermingled with the distributed cells (arrowhead) (original magnification ×2000).

SCANNING ELECTRON MICROSCOPY

The expanded ILMs were dehydrated in ethanol and water on a glass slide. The specimens were saturated in t-butyl alcohol, and critical-point drying (Eiko, Tokyo) was performed. The glass slide was cut into a 10-mm square. The specimens were then placed on stubs by means of self-adhering carbon tabs and sputtered with gold of 20-nm thickness by an argon plasma coater (Eiko).[36,37] The specimens were observed with a JSM 840 electron microscope (JEOL).

CELLULAR DISTRIBUTION ON THE ILM

Cellular distribution was observed in 23 specimens (stage 2 in 5 eyes, stage 3 in 8 eyes, and stage 4 in 10 eyes) (Table) by scanning electron microscopy, and the results were analyzed according to the macular hole staging proposed by Gass.[3,5,30] The distance from the top of the cellular distribution to the edge of the macular hole on the ILM was measured and analyzed using analysis software (MacScope; Mitani, Fukui, Japan). The results were expressed as means±SDs. The t test was used to calculate the probability by comparing data between the groups, and $P<.05$ was considered to be statistically significant.

RESULTS

VERTICAL ANALYSIS OF PEELED ILM

Light microscopical examination of semithin sections showed characteristic sinusoidal folds of complexly folded ILM (**Figure 1**A). Transmission electron microscopy
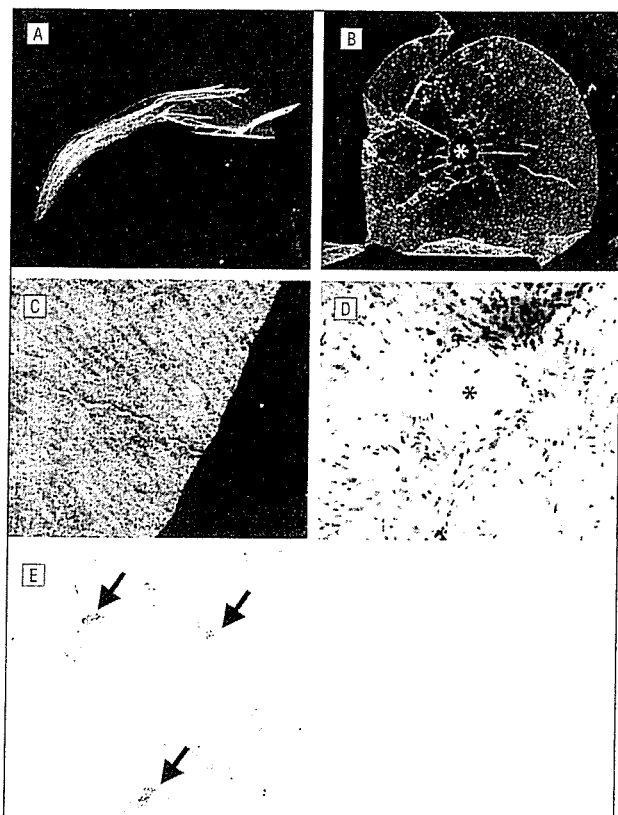
Figure 2. Topographic bird's-eye analysis of the internal limiting membrane (ILM) by light microscopy and fluorescence microscopy. The complexly folded excised ILM (A) extended onto a glass slide showed the intact ILM sheet containing an ILM defect corresponding to the area of the macular hole (asterisk) (B) (original magnification ×4). C, A dark-field illumination image showed that the ILM has the characteristic multilinear pattern associated with the underlying nerve fibers of the ganglion cells (original magnification ×10). D, The hematoxylin-eosin–stained section showed migrating cells around the macular hole (asterisk) (original magnification ×200). E, Some of the cells on the ILM were pigmented cells (arrows) (original magnification ×400).
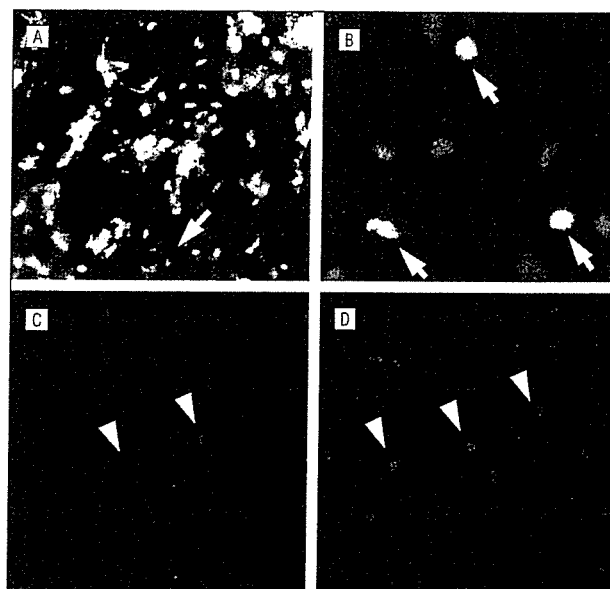

Figure 3. Immunohistochemical analysis of the distributed cells on the internal limiting membrane. A, Double immunohistochemistry of glial fibrillary acidic protein (green) and cytokeratin 18 (red) showed a mosaic-like migration pattern of glial fibrillary acidic protein–positive glial cells and cytokeratin 18–positive retinal pigment epithelial cells. Some of the cytokeratin 18–positive cells were pigmented (arrow) (original magnification ×200). B, Nuclear staining by 4',6-diamino-2-phenylindole dihydrochloride showed chromosomes of dividing nuclei (arrows) (original magnification ×1000). Immunohistochemistry of proliferating cell nuclear antigen (C) and Ki-67 (D) showed proliferating cells (arrowheads) among the distributed cells on the internal limiting membrane (original magnification ×400).

showed collagen membranous tissue with a smooth inner (vitreous) surface and an irregular outer (retinal) surface (Figure 1B). In the early stage of the macular hole (stage 2)', cellular migration was rarely seen (Figure 1B). Some cells, namely, glial cells, retinal pigment epithelial cells, and origin-unknown fibroblast-like cells, were seen on the inner surface of the ILM in the middle stages (stage 3) (Figure 1C) of the macular hole and were seen often in the later stages (stage 4) (Figure 1D). Some cellular membranes and organelles derived from underlying Muller cells were occasionally seen on the outer surface of the ILM; however, there were no changes according to the stage of development of the macular holes (Figure 1B-D). We could not identify the location of the macular hole in complexly folded ILM by ultrathin cross sections.

HORIZONTAL ANALYSIS OF EXPANDED ILM

Light microscopical examination of the excised whole ILM (Figure 2A) spread out onto a glass slide showed the intact ILM sheet containing a macular hole (Figure 2B). Dark-field illumination micrography showed that the ILM had the characteristic multilinear pattern associated with the underlying nerve fibers of the ganglion cells (Figure 2C). The hematoxylin-eosin–stained section showed migrat-

ing cells around the macular hole (stage 4) (Figure 2D). A few pigmented cells were seen among the distributing cells around the macular hole on the ILM (Figure 2E).

IMMUNOHISTOCHEMICAL ANALYSIS

Immunohistochemical analysis revealed that most of the dispersed cells on the ILM were glial fibrillary acidic protein–positive glial cells (Figure 3A). There were also cytokeratin 18–positive retinal pigment epithelial cells among the glial cells (Figure 3A). These cells formed a continuous cellular sheet around the macular hole on the ILM. To investigate whether these cells were migrating and/or proliferating on the ILM, we examined their proliferation by 2 different proliferating cell markers, PCNA and Ki-67. Proliferating cell nuclear antigen is a 36-kd proliferation-associated antigen, and Ki-67 is a large nuclear antigen preferentially expressed during all of the active phases of the cell cycle but absent in resting cells. Nuclear staining by 4',6-diamino-2-phenylindole dihydrochloride showed chromosomes of dividing nuclei (Figure 3B). Both PCNA and Ki-67 showed positive staining in the nucleus of the proliferating cells (Figure 3C and D). The PCNA-positive cells and Ki-67–positive cells accounted for 7% and 9%, respectively, of the total cells on the ILM. The proliferating cells dispersed around the distributed cells around the macular hole, and an obvious proliferating front was not observed in the specimens.

VERTICAL ANALYSIS OF EXPANDED ILM

Light microscopical examination of semithin sections of the expanded ILM showed a linear shape of the ILM

Figure 4. Vertical observation of the expanded internal limiting membrane (ILM). A, Light microscopical examination of a semithin section of the expanded ILM showed the linear shape of the ILM. On the expanded ILM, few Azur II–stained cells were seen around the ILM defect corresponding to the area of the stage 4 macular hole (asterisk) (original magnification ×600). Transmission electron microscopy showed the expanded linear ILM and migrating cells (original magnification ×2000) (B) as well as dense collagen fibers, namely, residual posterior vitreous hyaloid between the ILM and migrating cells (original magnification ×6600) (C).

Figure 5. Topographic analysis of the internal limiting membrane (ILM) by scanning electron microscopy. Scanning electron microscopy revealed a smooth inner surface of the excised ILM, where migrating cells from the macular hole were rarely seen in the early stage (stage 2) of development of the macular hole (A), and revealed a rough outer surface of the excised ILM (B) (original magnification ×3000). Migrating cells from the macular hole were more prominent in the later stage (stage 4) of development of the macular hole (original magnification ×1800) (C), showing flat and sticking morphological features and spreading filopodia on the ILM (original magnification ×8000) (D). E, A topographic bird's-eye view of the expanded ILM showed no cellular migration around the ILM defect corresponding to the area of the stage 2 macular hole (asterisk) (original magnification ×75).

(**Figure 4**A). On the expanded ILM, few Azur II–stained cells were shown around the ILM defect corresponding to the area of the macular hole at stage 4, providing better spatial understanding of the ILM. Transmission electron microscopy demonstrated the expanded linear ILM and migrating cells (Figure 4B) as well as dense collagen fibers, namely, residual posterior hyaloid between the ILM and migrating cells (Figure 4C).

SCANNING ELECTRON MICROSCOPY

Scanning electron microscopy revealed a smooth inner surface (**Figure 5**A) and rough outer surface (Figure 5B) of the ILM. This dense collagen layer is a basement membrane of Muller cells, namely, the ILM, and demonstrates the characteristic smooth surface. Neither fibrous collagen nor fibrillar vitreous collagen are smooth surfaced by scanning electron microscopy. In the early stages of development of the macular hole, migrating cells were not apparent on the inner surface of the ILM around the macular hole (Figure 5A). Notably, in the later stages, migrating cells were clearly visible around the ILM defect corresponding to the area of the macular hole (Figure 5C), indicating that these cells were migrating away from the macular hole. Cellular migration occurred on the ILM, showing flat and sticking morpho-
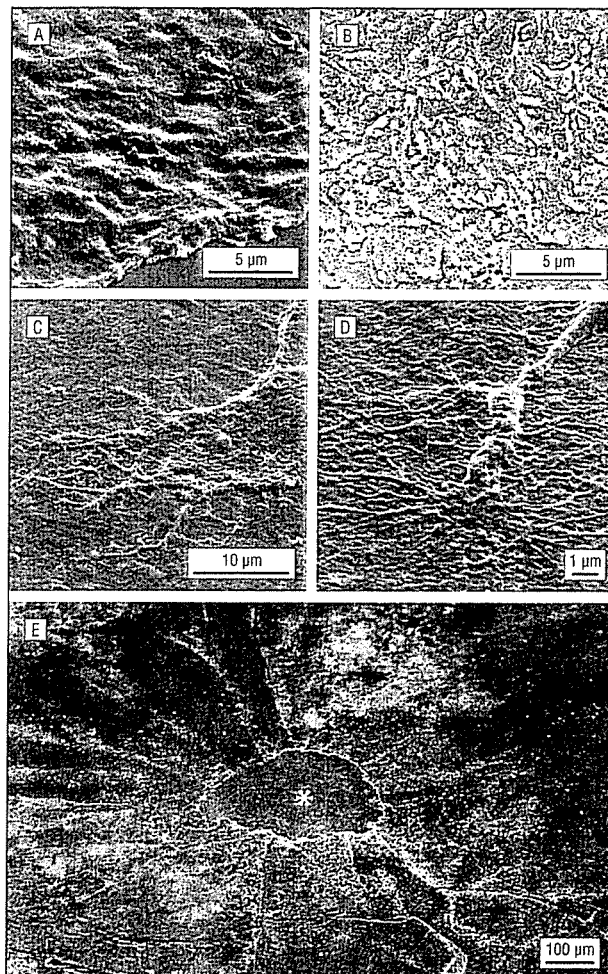
logical features and spreading filopodia on the ILM (Figure 5D). A topographic image of the expanded ILM showed no cellular migration around the ILM defect corresponding to the area of the macular hole at stage 2 (Figure 5E).

CELLULAR MIGRATION FROM THE MACULAR HOLE

The distance of cellular migration from the ILM defect corresponding to the area of the macular hole gradually increased through each stage of development of the macular hole (**Figure 6**). The cellular migration occurred from the edge of the macular hole and developed to the peripheral area of the ILM (Figure 6A-C). In most cases, cellular migration was observed as a continuous sheet of cells around the macular hole (Figure 6B and C).
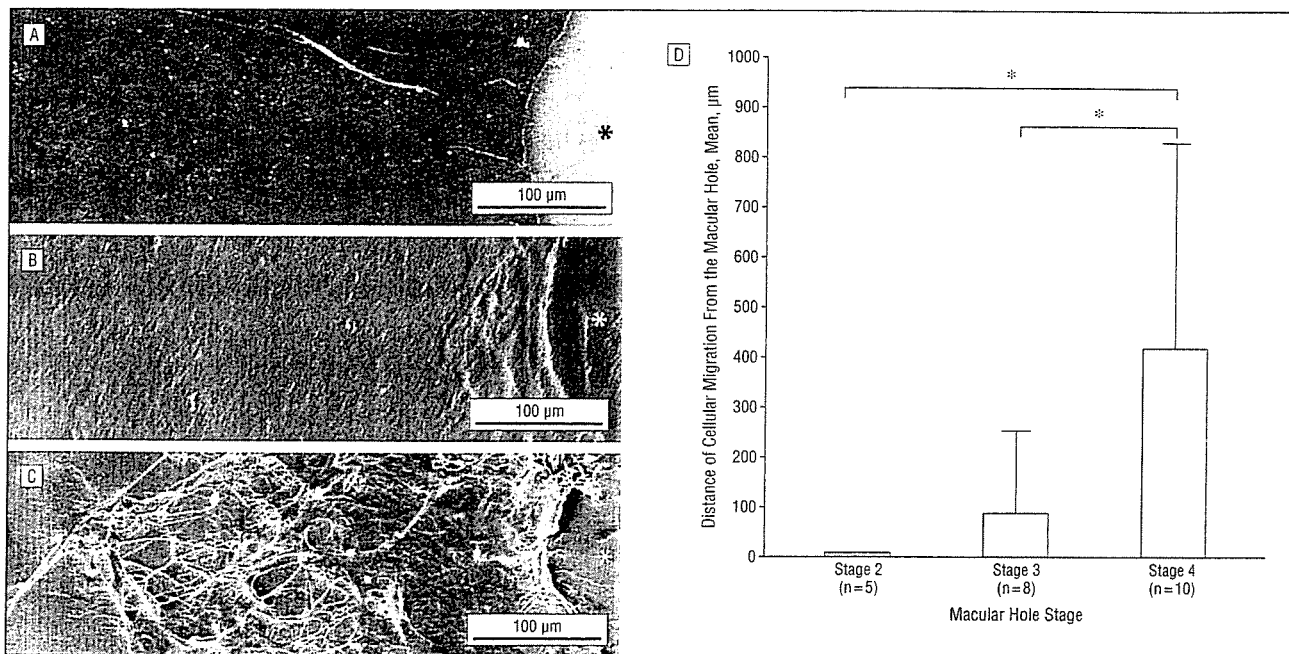
Figure 6. Quantitative analysis of cellular migration from the macular hole. The representative developmental stages of cellular migration on the internal limiting membrane from the internal limiting membrane defect corresponding to the area of the macular hole (asterisks) are shown for stage 2 (A), stage 3 (B), and stage 4 (C) (original magnification ×140). D, The distance of cellular migration from the edge of the macular hole was measured and analyzed using analysis software (MacScope; Mitani, Fukui, Japan). The *t* test was used to calculate the probability by comparing data between the groups, and $P<.05$ was considered to be statistically significant (asterisks). The area of cellular migration gradually enlarged as the macular hole passed through the later stages of development. Error bars indicate SDs.

COMMENT

This study demonstrates that cellular migration around the macular hole develops after the macular break occurs and that cellular migration occurs from the macular hole and enlarges on the ILM. To our knowledge, this is the first article clearly showing that cellular migration on the ILM is not necessary for the initial formation of a macular break.

COMPREHENSIVE TOPOGRAPHIC ANALYSIS OF EXCISED ILM

Some previous histological studies[26-28] demonstrated cellular migration on the ILM around the macular hole; however, this was based on findings from the ultrathin partial cross sections of the ILM, leaving the origin and distribution of the cells largely unknown, as shown in Figure 1. We propose a topographic analysis of the whole excised ILM that enables understanding of cellular migration, especially its origin, frequency, distribution, and relationship with the macular hole (Figure 6). Whereas a cross section gives a snapshot of a limited area of excised complexly folded ILM at a particular time point (Figure 1), horizontal observation enables a comprehensive analysis of spatial distribution that offers a temporal perspective of cellular migration around a macular hole in its process of development (Figure 6).

DISTRIBUTED CELLS AROUND THE MACULAR HOLE

The ultrastructural studies[23,27,28,38] of migrating cells and epiretinal membranes have found them to be glial cells, reti-

nal pigment epithelium, myofibroblasts, and so on. Our light microscopical studies demonstrate that some of the migrating cells were pigmented cells (Figure 2E), and immunohistochemical studies also demonstrate a mosaic-like migration pattern of glial fibrillary acidic protein–positive glial cells and cytokeratin 18–positive retinal pigment epithelial cells (Figure 3A). These cells were intermingled to form an epiretinal membrane as a continuous cellular sheet on the ILM (Figure 2E, Figure 3A, Figure 4B, and Figure 5C). To further estimate the cellular proliferation on the ILM, we examined their proliferation by 2 different proliferating cell markers, PCNA and Ki-67. Although the proliferating cells dispersed around the distributed cells around the macular hole, an obvious proliferating front was not observed in the specimens.

ROLE OF CELLULAR MIGRATION IN THE PATHOGENESIS OF THE MACULAR HOLE

Figure 6A shows a complete lack of cellular migration in the early stage (stage 2) of development of the macular hole. In contrast, Figure 6B shows cellular development around the edge of the macular hole, and Figure 6C shows a large amount of cellular migration from the macular hole to the peripheral area. Notably, in the later stage of development of the macular hole, some specimens showed no cellular migration around the macular hole (Table). Our results confirm that the initial break of the macular hole is not dependent on cellular migration around the macular hole (Figure 6D). In contrast, cellular migration developed after the macular break and expanded from the edge of the macular hole to the periphery (Figure 4A and Figure 6A-C), finally forming an

epiretinal membrane on the ILM. This cellular migration and its contraction of the extracellular matrix on the ILM (Figure 1B-D and Figure 4) might lead to further progression of the macular hole (stage 3) and might keep the macular hole open even after PVD (stage 4).

The role of cellular migration in the pathogenesis of the macular hole remains quite unclear. We provide a comprehensive bird's-eye analysis of the ultrastructure of the ILM and demonstrate cellular migration and proliferation in a quantitative manner, proposing the association of cellular migration to the pathogenesis of a macular hole.

REFERENCES

1. Avila MP, Jalkh AE, Murakami K, Trempe CL, Schepens CL. Biomicroscopic study of the vitreous in macular breaks. *Ophthalmology*. 1983;90:1277-1283.
2. Kakehashi A, Schepens CL, Trempe CL. Vitreomacular observations, I: vitreomacular adhesion and hole in the premacular hyaloid. *Ophthalmology*. 1994; 101:1515-1521.
3. Gass JD. Idiopathic senile macular hole: its early stages and pathogenesis. *Arch Ophthalmol*. 1988;106:629-639.
4. Johnson RN, Gass JD. Idiopathic macular holes: observations, stages of formation, and implications for surgical intervention. *Ophthalmology*. 1988;95:917-924.
5. Gass JD. Reappraisal of biomicroscopic classification of stages of development of a macular hole. *Am J Ophthalmol*. 1995;119:752-759.
6. Gass JD. Muller cell cone, an overlooked part of the anatomy of the fovea centralis: hypotheses concerning its role in the pathogenesis of macular hole and foveomacular retinoschisis. *Arch Ophthalmol*. 1999;117:821-823.
7. Kishi S, Shimizu K. Posterior precortical vitreous pocket. *Arch Ophthalmol*. 1990; 108:979-982.
8. Kishi S, Hagimura N, Shimizu K. The role of the premacular liquefied pocket and premacular vitreous cortex in idiopathic macular hole development. *Am J Ophthalmol*. 1996;122:622-628.
9. Kishi S, Takahashi H. Three-dimensional observations of developing macular holes. *Am J Ophthalmol*. 2000;130:65-75.
10. Dugel PU, Smiddy WE, Byrne SF, Hughes JR, Gass JD. Macular hole syndromes: echographic findings with clinical correlation. *Ophthalmology*. 1994; 101:815-821.
11. Johnson MW, Van Newkirk MR, Meyer KA. Perifoveal vitreous detachment is the primary pathogenic event in idiopathic macular hole formation. *Arch Ophthalmol*. 2001;119:215-222.
12. Bartsch DU, Intaglietta M, Bille JF, Dreher AW, Gharib M, Freeman WR. Confocal laser tomographic analysis of the retina in eyes with macular hole formation and other focal macular diseases. *Am J Ophthalmol*. 1989;108:277-287.
13. Weinberger D, Stiebel H, Gaton DD, Priel E, Yassur Y. Three-dimensional measurements of idiopathic macular holes using a scanning laser tomograph. *Ophthalmology*. 1995;102:1445-1449.
14. Beausencourt E, Elsner AE, Hartnett ME, Trempe CL. Quantitative analysis of macular holes with scanning laser tomography. *Ophthalmology*. 1997;104:2018-2029.
15. Puliafito CA, Hee MR, Lin CP, et al. Imaging of macular diseases with optical coherence tomography. *Ophthalmology*. 1995;102:217-229.
16. Gaudric A, Haouchine B, Massin P, Paques M, Blain P, Erginay A. Macular hole formation: new data provided by optical coherence tomography. *Arch Ophthalmol*. 1999;117:744-751.
17. Takahashi H, Kishi S, Ebato K, Hagimura N, Shimizu K, Kamei Y. Tomographic features of a lamellar macular hole formation and a lamellar hole that progressed to a full-thickness macular hole. *Am J Ophthalmol*. 2000;130:677-679.
18. Spaide RF, Wong D, Fisher Y, Goldbaum M. Correlation of vitreous attachment and foveal deformation in early macular hole states. *Am J Ophthalmol*. 2002; 133:226-229.
19. Uemoto R, Yamamoto S, Aoki T, Tsukahara I, Yamamoto T, Takeuchi S. Macular configuration determined by optical coherence tomography after idiopathic macular hole surgery with or without internal limiting membrane peeling. *Br J Ophthalmol*. 2002;86:1240-1242.
20. Sato H, Kawasaki M, Yamashita H. Observation of idiopathic full-thickness macular hole closure in early postoperative period as evaluated by optical coherence tomography. *Am J Ophthalmol*. 2003;136:185-187.
21. Drexler W, Sattmann H, Hermann B, et al. Enhanced visualization of macular pathology with the use of ultrahigh-resolution optical coherence tomography. *Arch Ophthalmol*. 2003;121:695-706.
22. Guyer DR, Green WR, de Bustros S, Fine SL. Histopathologic features of idiopathic macular holes and cysts. *Ophthalmology*. 1990;97:1045-1051.
23. Yooh HS, Brooks HL Jr, Capone A Jr, L'Hernault NL, Grossniklaus HE. Ultrastructural features of tissue removed during idiopathic macular hole surgery. *Am J Ophthalmol*. 1996;122:67-75.
24. Hirayama K, Hata Y, Noda Y, et al. The involvement of the rho-kinase pathway and its regulation in cytokine-induced collagen gel contraction by hyalocytes. *Invest Ophthalmol Vis Sci*. 2004;45:3896-3903.
25. Frangieh GT, Green WR, Engel HM. A histopathologic study of macular cysts and holes. *Retina*. 1981;1:311-336.
26. Smiddy WE, Michels RG, de Bustros S, de la Cruz Z, Green WR. Histopathology of tissue removed during vitrectomy for impending idiopathic macular holes. *Am J Ophthalmol*. 1989;108:360-364.
27. Messmer EM, Heidenkummer HP, Kampik A. Ultrastructure of epiretinal membranes associated with macular holes. *Graefes Arch Clin Exp Ophthalmol*. 1998; 236:248-254.
28. Kampik A, Green WR, Michels RG, Nase PK. Ultrastructural features of progressive idiopathic epiretinal membrane removed by vitreous surgery. *Am J Ophthalmol*. 1980;90:797-809.
29. Rosa RH Jr, Glaser BM, de la Cruz Z, Green WR. Clinicopathologic correlation of an untreated macular hole and a macular hole treated by vitrectomy, transforming growth factor-beta 2, and gas tamponade. *Am J Ophthalmol*. 1996;122: 853-863.
30. Gass JD. Idiopathic senile macular hole: its early stages and pathogenesis. 1988. *Retina*. 2003;23:629-639.
31. Enaida H, Hata Y, Ueno A, et al. Possible benefits of triamcinolone-assisted pars plana vitrectomy for retinal diseases. *Retina*. 2003;23:764-770.
32. Sakamoto T, Miyazaki M, Hisatomi T, et al. Triamcinolone-assisted pars plana vitrectomy improves the surgical procedures and decreases the postoperative blood-ocular barrier breakdown. *Graefes Arch Clin Exp Ophthalmol*. 2002;240:423-429.
33. Matsumoto H, Enaida H, Hisatomi T, et al. Retinal detachment in morning glory syndrome treated by triamcinolone acetonide-assisted pars plana vitrectomy. *Retina*. 2003;23:569-572.
34. Sonoda KH, Sakamoto T, Enaida H, et al. Residual vitreous cortex after surgical posterior vitreous separation visualized by intravitreous triamcinolone acetonide. *Ophthalmology*. 2004;111:226-230.
35. Hisatomi T, Sakamoto T, Murata T, et al. Relocalization of apoptosis-inducing factor in photoreceptor apoptosis induced by retinal detachment in vivo. *Am J Pathol*. 2001;158:1271-1278.
36. Hisatomi T, Sakamoto T, Sonoda KH, et al. Clearance of apoptotic photoreceptors: elimination of apoptotic debris into the subretinal space and macrophage-mediated phagocytosis via phosphatidylserine receptor and integrin alphavbeta3. *Am J Pathol*. 2003;162:1869-1879.
37. Nakamura T, Murata T, Hisatomi T, et al. Ultrastructure of the vitreoretinal interface following the removal of the internal limiting membrane using indocyanine green. *Curr Eye Res*. 2003;27:395-399.
38. Campochiaro PA, Van Niel E, Vinores SA. Immunocytochemical labeling of cells in cortical vitreous from patients with premacular hole lesions. *Arch Ophthalmol*. 1992;110:371-377.